*Desalination and Water Treatment*
www.deswater.com

doi: 10.1080/19443994.2016.1138897

57 (2016) 24200–24209
November

Taylor & Francis
Taylor & Francis Group

# Adsorption of zinc ions on bone char using helical coil-packed bed columns and its mass transfer modeling

J. Moreno-Pérez[a], A. Bonilla-Petriciolet[a,*], C.K. Rojas-Mayorga[a], D.I. Mendoza-Castillo[b], M. Mascia[c], M. Errico[d]

[a]*Departamento de Ingeniería Química, Instituto Tecnológico de Aguascalientes, Aguascalientes 20256, Mexico, email: jaime_morp@hotmail.com (J. Moreno-Pérez), Tel. +52 4499105002; emails: petriciolet@hotmail.com (A. Bonilla-Petriciolet), karymayorga@yahoo.com.mx (C.K. Rojas-Mayorga)*
[b]*Cátedras CONACYT – Instituto Tecnológico de Aguascalientes, Aguascalientes 20256, Mexico, email: didi_men@hotmail.com*
[c]*Dipartimento di Ingegneria Meccanica Chimica e del Materiali, Università degli Studi di Cagliari, Cagliari 09123, Italy, email: michele.mascia@dimcm.unica.it*
[d]*Department of Chemical Engineering, Biotechnology and Environmental Technology, University of Southern Denmark, Campusvej 55, DK-5230 Odense M, Denmark, email: maer@kbm.sdu.dk*

Received 26 October 2015; Accepted 31 December 2015

ABSTRACT

This study reports the assessment of helical coil-packed bed columns for $Zn^{2+}$ adsorption on bone char. $Zn^{2+}$ adsorption breakthrough curves have been obtained using helical coil columns with different characteristics and a comparison has been conducted with respect to the results of straight fixed-bed columns. Results showed that the helical coil adsorption columns may offer an equivalent removal performance than that obtained for the traditional packed bed columns but using a compact structure. However, the coil diameter, number of turns, and feed flow appear to be crucial parameters for obtaining the best performance in this packed-bed geometry. A mass transfer model for a mobile fluid flowing through a porous media was used for fitting and predicting the $Zn^{2+}$ breakthrough curves in helical coil bed columns. Results of adsorbent physicochemical characterization showed that $Zn^{2+}$ adsorption on bone char can be attributed to an ion-exchange mechanism. In summary, helical coil columns appear to be a feasible configuration for large-scale adsorption systems with high flow rates where a significant reduction on purification system size can be obtained without compromising the adsorbent performance.

*Keywords:* Helical coil-packed columns; Adsorption; Bone char; Zinc; Mass transfer model

## 1. Introduction

Adsorption processes are widely used in industrial applications including the purification and treatment of wastewaters and the production of drinking water. Fixed-bed column is the most common configuration for large-scale adsorption systems especially using granular activated carbon [1–3], which is considered as the most effective and economical adsorbent for water treatment [4–7]. The design of dynamic adsorption systems must take into account several parameters such as: adsorbent size and distribution, fluid flow rate, solute concentration, etc. In fact, the

*Corresponding author.

breakthrough curve that characterizes the dynamic adsorption process is a function of both the operating conditions and bed geometry [8]. Theoretically, the adsorption columns can be designed for operating at different scenarios and the flexibility and low energy requirements are the main reasons for its widespread usage in water treatment and purification.

For developing countries, it is relevant to reduce the costs associated with the design, building, and operation of water purification systems. The treatment of fluids with high flow rates or high pollutant contents usually requires adsorption columns with large bed heights to improve the adsorbent performance and to reach the desirable concentration limits in the treated effluent [9]. Dynamic systems of multiple columns are commonly used and they involve sequential arrangements of two or more fixed beds. Although several adsorption columns can be connected in series to satisfy the design conditions, the cost and size of separation system are critical factors that limit the quantity of beds operated at this configuration [10]. Therefore, compact structures are desirable to reduce the dimension of purification systems and to have less installation, maintenance and repair costs, without causing an adverse effect on the adsorbent performance. One option for reaching this target in large-scale water treatment systems implies modifications in the packed-bed geometry. In particular, previous studies have reported that alternative bed geometries can be used for packed-bed columns [2,10–12]. For example, Pota and Mathews [10] reported the adsorption of trichloroethylene on activated carbon using tapered convergent beds, while Sze et al. [2] and Sze and McKay [11,12] studied the application of tapered adsorption columns for the removal of acid dye yellow 117 and para-chlorophenol on activated carbon. Results of these studies showed that it is feasible to enhance the adsorbent utilization in dynamic systems via the bed geometry/configuration. However, these studies did not address the key point of adsorption system size, which is a condition that may limit the system implementation in real-life operating scenarios. Based on this fact, others packed-bed configurations should be studied and analyzed to intensify the dynamic adsorption processes for wastewater treatment.

It is important to highlight that the helical coil configurations have found extensive use in industrial applications including power generation, nuclear industry, refrigeration, and food industry [13]. In view of the analogy between heat and mass transfers, the helical coil geometry for adsorption columns may offer some operational advantages compared to straight bed columns. Specifically, the helical coil bed configuration offers a compact structure for the water treatment system besides the flow in curve pipes is more stable than flow in straight pipes. However, the applications of helical columns have been mainly focused on the improvement of heat transfer. Some studies have reported the application of helical coil configurations to improve mass transfer rates in reverse osmosis units or membrane blood oxygenators [14]. But, to the best of author's knowledge, this configuration has not been applied in adsorption processes. So, it would be interesting to analyze the capabilities and limitations of the application of this bed geometry in adsorption systems for water treatment.

In this study, the liquid-phase adsorption of $Zn^{2+}$ ions on bone char at helical coil bed columns has been analyzed. $Zn^{2+}$ is a priority pollutant on the context of wastewater treatment due to its toxicological effects on human beings [7,15,16]. Preliminary results indicated that bone char is a promising adsorbent for $Zn^{2+}$ removal from aqueous solution at batch reactors [17]. A comparison of breakthrough curves of helical coil columns for $Zn^{2+}$ adsorption on bone char and those obtained for straight packed columns has been performed. In addition, a mass transfer model was used for breakthrough curve data correlation. This study is the first attempt to analyze the potential application of helical coil configurations in adsorption columns for the removal of priority water pollutants.

## 2. Methodology

### 2.1. Description and physicochemical characterization of bone char used for $Zn^{2+}$ removal

Commercial bone char provided by a Mexican company was used in this study, which has been synthesized from the thermal treatment of bovine bone wastes. Bone char was washed with deionized water, dried, and sieved for $Zn^{2+}$ adsorption experiments. The main textural parameters of this adsorbent were determined using nitrogen adsorption–desorption isotherms at 77 K. They include: BET surface area of 74 $m^2$, micropore volume of 0.027 $cm^3/g$ (28%), mesopore volume of 0.067 $cm^3/g$ (72%), and total pore volume of 0.094 $cm^3/g$, respectively. The functional groups of this adsorbent were determined using transmission FTIR spectra recorded on a Bruker IFS 66/S spectrophotometer and the adsorbent samples were analyzed using spectroscopic-grade KBr. Analysis was performed using a sample scan time of 200 scans and a resolution of 4 $cm^{-1}$. The adsorbent crystalline structure was studied using an X-ray diffractometer Bruker D8-Advance with a Göebel mirror, a tube of

RX with copper anode and radiation Cu Ka ($k$ = 1.5406 Å). Diffractograms were obtained at $10 \leq 2\theta \leq 80$ and the database used for analysis was from International Center for Diffraction Data (ICDD). The elemental composition was determined by X-ray fluorescence (XRF) analysis, which was performed using a sequential X-ray spectrometer equipped with a rhodium tube and beryllium window. X-ray photoelectron spectroscopy (XPS) was used to estimate the $Zn^{2+}$ content at the adsorbent surface after adsorption experiments. This analysis was performed with a Prevac photoelectron spectrometer equipped with a hemispherical analyzer (VG Scienta R3000). Spectra were taken using a mono-chromatized aluminum source Al Kα ($E$ = 1486.6 eV). The base pressure in the analytical chamber was $5 \times 10^{-9}$ mbar. The binding energy signal was calibrated using the Au 4f7/2 line of a cleaned gold sample at 84.0 eV. The adsorbent surface composition was estimated employing the areas and binding energies of O 1s, P 2p, Ca 2p, and Zn 2p core levels, respectively.

### 2.2. Dynamic adsorption experiments using helical coil-packed bed columns

Breakthrough curves for $Zn^{2+}$ adsorption on bone char were obtained at different operating conditions of helical coil columns. Fig. 1 shows the configuration and terminology used for helical coil pipes. Note that the curved shape of this bed geometry causes the fluid to experience centrifugal force, which will depend on the fluid velocity and the curvature of the coil. Therefore, counter-rotating vortices are generated, called secondary flows [18], which may produce additional transport of the solution over the cross-section of the column. In particular, we have analyzed two relevant parameters of helical coil columns on the adsorption performance of bone char. These parameters are the coil diameter and the number of turns for the coil column. A polyurethane-based pipe was used as the building material for helical coil columns. The pipe diameter (i.e. internal bed diameter) was kept at ≈ 0.7 cm and the helical coil columns consisted of 3 and 6 turns. These turns corresponded to coil diameters of 10 and 4.2 cm, respectively, which were measured between the centers of the pipes. On the other hand, the coil pitch (i.e. the distance between two adjacent turns) for all experiments was zero with the objective of obtaining a compact adsorption column.

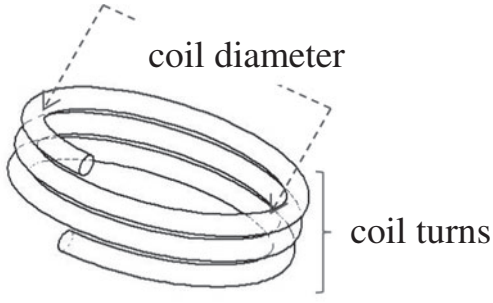


Fig. 1. Illustration and nomenclature of a helical coil pipe.

Adsorption experiments were performed using feed solutions with $Zn^{2+}$ concentrations of 24, 48, and 100 mg/L at feed flows of 6.5 and 13 mL/min, which were obtained with a peristaltic pump. These feed flows correspond to residence times of ~3 and 1.5 min, respectively. Metal solutions were prepared using hydrated zinc nitrate (J.T. Baker) and deionized water. All fixed-bed experiments were performed at 30˚C and pH 5 using 33.25 g of bone char with a mean particle diameter of 0.67 mm (i.e. a bed length of 98 cm). Bone char was packed into the columns and, after packing, deionized water was fed to the columns for 2 h, at the selected operating conditions, to wet the adsorbent and to expel the air. Samples of column outlet were collected for determining the breakthrough curves of $Zn^{2+}$ adsorption on bone char and the metal concentrations were quantified using atomic absorption spectroscopy with an iCE 3300 Thermo Scientific spectrometer. For comparison, the $Zn^{2+}$ adsorption experiments were performed using a conventional straight packed-bed column. Specifically, the breakthrough curves were obtained at the operating conditions (i.e. adsorbent mass, feed flows, and metal concentrations) used for helical coil-bed columns. This comparison was performed to identify the capabilities and limitations of using this alternative bed configuration for dynamic adsorption processes.

Data analysis of breakthrough curves included the calculation of the breakthrough points, $[Zn^{2+}]_{outlet} = w \cdot [Zn^{2+}]_{feed}$ where $w \in (0,1)$, and the estimation of the bone char adsorption capacities $q_{bchar}$. The adsorption capacities of bone char were calculated from the graphical integration of the experimental breakthrough curves using:

$$q_{bchar} = \int_{t=0}^{t=t_{oper}} \left( \frac{[Zn^{2+}]_{feed} - [Zn^{2+}]_{outlet}}{m_{ads}} \right) Q \, dt \qquad (1)$$

where $Q$ is the feed flow, $m_{ads}$ is the adsorbent amount used in packed columns, and $t$ is the operating time of dynamic adsorption experiments, respectively. A Matlab® program was employed for this calculation using the trapezoid rule.

### 2.3. Mass transfer modeling of breakthrough curves

There are various approaches for modeling mass transfer mechanisms in packed-bed adsorption columns [19], which show different mathematical complexity. In this study, a mass transfer model for a mobile fluid flowing through a porous media was applied for data modeling of $Zn^{2+}$ breakthrough curves using bone char and helical coil columns. This model has been used as a first step to obtain a mathematical approach that can predict the performance of these adsorption columns. Based on the fact that the axial dispersion is commonly higher than the diffusion in packed bed columns [20], the mass transfer model is given by [21]:

$$\varepsilon\frac{\partial c}{\partial t}+\rho_b\frac{\partial q_{bed}}{\partial t}+\nabla\cdot(cu)=\nabla\cdot(D_D\nabla c) \tag{2}$$

where $\varepsilon$ is the porosity or bed void fraction, $\rho_b$ is the bulk density in kg/m$^3$, $t$ is the operation time in h, $D_D$ is the axial dispersion coefficient in m$^2$/s, $c = [Zn^{2+}]$ is the adsorbate concentration in the fluid phase given in mol/m$^3$, $q_{bed}$ is the bed adsorption capacity in mol/kg, and $u$ is the fluid velocity in m/s, respectively. Applying a variable change for $q_{bed}$, we have:

$$\frac{\partial q_{bed}}{\partial t}=\frac{\partial q_{bed}}{\partial c}\frac{\partial c}{\partial t} \tag{3}$$

where $K_p = \partial q_{bed}/\partial c$ is an adsorption constant given in m$^3$/kg and $x$ is the distance along the bed length, respectively. Combining the equations and assuming that the change of adsorbate concentration occurs in space variable $x$, the final mass transfer model is defined as:

$$(\varepsilon+\rho_b K_p)\frac{\partial c}{\partial t}+u\frac{\partial c}{\partial x}=D_D\frac{\partial^2 c}{\partial x^2} \tag{4}$$

In this model, the parameters $K_P$ and $D_D$ are determined via the data fitting of experimental breakthrough curves. The initial and boundary conditions for this model are [8,20]:

$$\begin{array}{lll} t=0, & 0<x<L, & c=0 \\ t>0, & x=0, & c=c_f \\ t>0, & x=L, & \frac{\partial c}{\partial x}\big|_{x=L}=0 \end{array} \tag{5}$$

where $L$ is the bed length and $c_f$ is the final concentration of outlet column obtained in experimental breakthrough curves. The differential equation governing the mass transfer in adsorption columns was solved using Comsol Multyphysics®. Parameters used for breakthrough data modeling are reported in Table 1 and the best values of $K_p$ and $D_D$ were determined one-at-a-time via a parametric study using this software.

## 3. Results

Fig. 2(a)–(f) shows the breakthrough curves of $Zn^{2+}$ adsorption on bone char using the helical coil bed columns for tested feed flows and metal concentrations. The shape and characteristics of the breakthrough curves are functions of these operating parameters and, consequently, they determine the dynamic performance of adsorption columns. As expected, the sharpness of $Zn^{2+}$ breakthrough curves increased with feed flow and inlet metal concentration. These results also confirmed that $Zn^{2+}$ adsorption breakthrough curves depend on the characteristics of helical coil columns. Specifically, the coil diameter and the number of turns affected the performance of metal adsorption. But, their effects on metal removal depend on the operating conditions of the bone char columns. For the lower feed flow, the effect of coil diameter and turns is more significant especially for the inlet metal concentrations of 24 and 48 mg/L, see Fig. 2(a) and (b). Note that helical coil columns with 6 turns (i.e. with the lower coil diameter) offered the best performance for $Zn^{2+}$ adsorption on bone char at the lower feed flow. Breakthrough curves for helical columns with 6 turns are more delayed and sharper than those for adsorption columns with 3 turns. But, at the upper feed flow, the change in coil diameter and turns does not provide a pronounced effect on the bed metal uptakes independent of the inlet $Zn^{2+}$ concentration, see Figs. 2(d)–(f). At this flow condition, breakthrough curves obtained for different coil turns are practically

Table 1
Parameters used in the mass transfer model for breakthrough data correlation of $Zn^{2+}$ adsorption on bone char

| Parameter | Value[a] |
|---|---|
| Bed void fraction ($\varepsilon$) | 0.3 |
| Bulk density $\rho_b$ (g/cm$^3$) | 1.2 |
| Solution density (g/cm$^3$) | 0.9956 |
| Solution viscosity (cp) | 0.7982 |
| Solvent molecular weight (g/mol) | 18 |
| Solute density (g/cm$^3$) | 7.1386 |
| Solute molecular weight (g/mol) | 65.93 |
| Solute volume (cm$^3$/mol) | 9.16 |

[a]Values obtained from database of Comsol Multyphysics® with except of $\varepsilon$ and $\rho_b$.

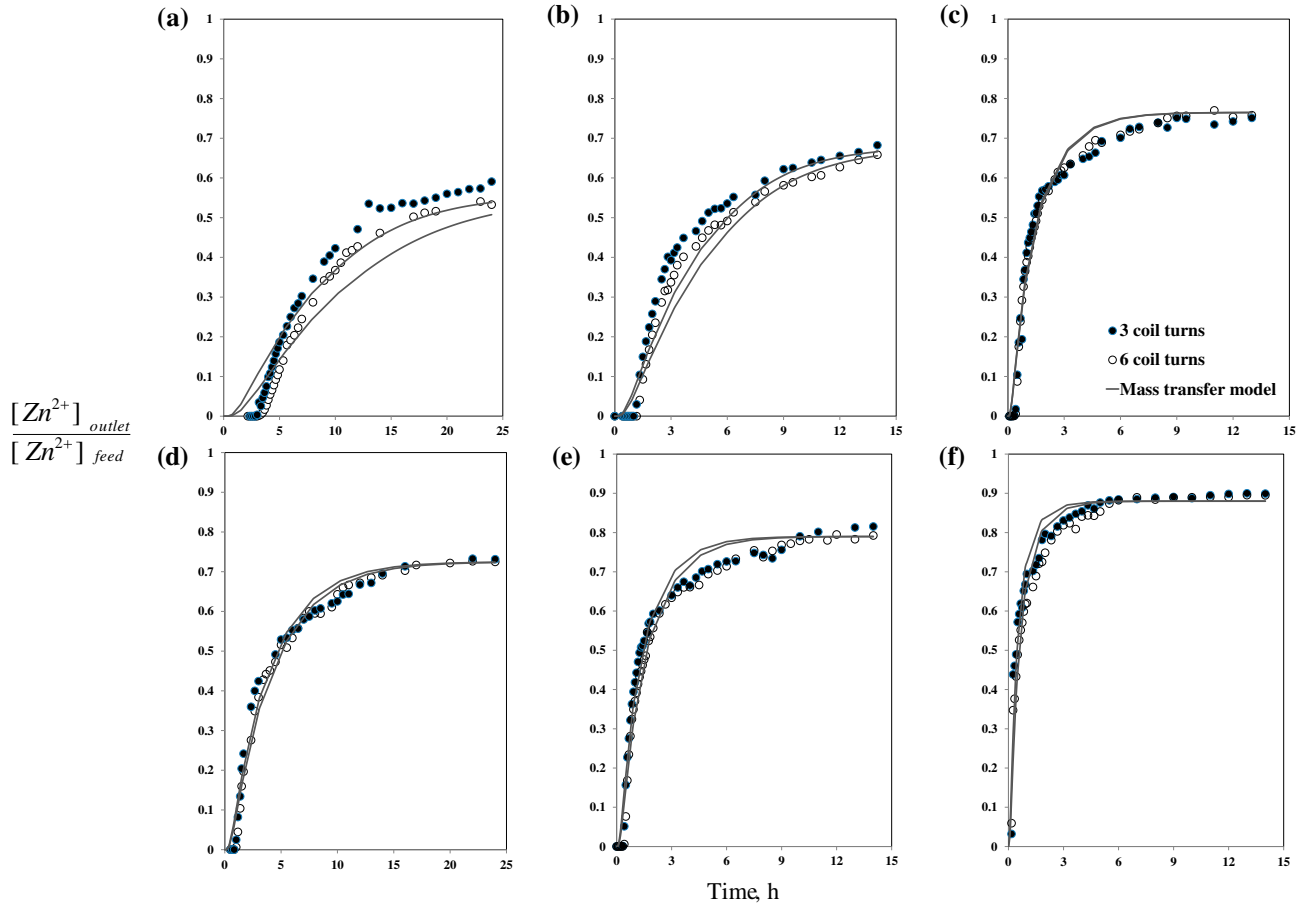


Fig. 2. Breakthrough curves for $Zn^{2+}$ adsorption on bone char using helical coil-packed columns. Metal concentration and feed flow: (a) 24 mg/L and 6.5 mL/min, (b) 48 mg/L and 6.5 mL/min, (c) 100 mg/L and 6.5 mL/min, (d) 24 mg/L and 13 mL/min, (e) 48 mg/L, and 13 mL/min, and (f) 100 mg/L and 13 mL/min.

equivalent. In helical coil configurations, the solution flowing through curved tubes induces a secondary flow where its intensity depends on the coil diameter and turns besides the feed flow [18]. Therefore, this secondary flow may improve the mixing inside the column and contribute to the mass transfer [14] depending of the operating conditions of dynamic adsorption process. In fact, results showed that the feed flow rate is a crucial parameter for the operation of helical coil adsorption columns.

Adsorption breakthrough curves obtained for conventional packed-bed columns are reported in Figs. 3(a) and (b), and the main parameters of $Zn^{2+}$ dynamic adsorption are reported in Table 2. Breakthrough data for helical coil columns were compared with those obtained for traditional straight packed bed adsorption columns for tested operating conditions. Overall, the straight fixed-bed column and the helical coil column with 6 turns showed a similar adsorption performance and, hence, similar breakthrough curves for $Zn^{2+}$ removal independent of metal concentration and feed flow. The breakthrough points and the bone char adsorption capacities of both conventional and six-turn helical beds are practically equivalent; see results of Table 2. Metal uptakes ranged from 4.0 to 6.0 mg/g where the three-turn helical coil columns showed the lowest $Zn^{2+}$ adsorption capacities and the shortest breakthrough points for all operating conditions. In particular, the order of breakthrough times is: conventional column ≈ six-turn helical column > - three-turn helical column. Then, the helical coil column with six turns is the best choice when considering the adsorbent performance and the size of purification system. Usually, the concentration of column outlet increases rapidly after reaching the breakthrough point. However, results reported in Figs. 2 and 3 show a region where the concentration profile is flat probably due to a relatively low $Zn^{2+}$ uptake by bone char. It is convenient to remark the $Zn^{2+}$ adsorption capacity of bone char is 23.0 mg/g at

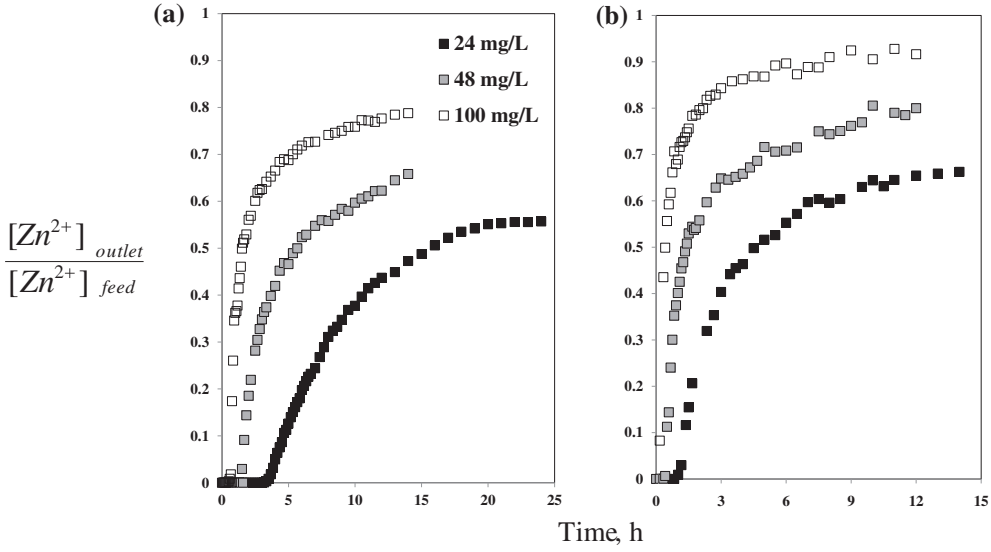


Fig. 3. Breakthrough curves for $Zn^{2+}$ adsorption on bone char using conventional (i.e. straight) packed columns. Feed flow: (a) 6.5 mL/min and (b) 13 mL/min.

Table 2
Breakthrough points, $Zn^{2+}$ adsorption capacities, and bed utilization for both conventional and helical coil adsorption columns

| | Operating conditions | | Breakthrough point[a] (h) | | | |
|---|---|---|---|---|---|---|
| Feed flow (mL/min) | $[Zn^{2+}]_{feed}$ (mg/L) | Bed geometry | $w$ = 0.05 | $w$ = 0.10 | $q_{bchar}$ (mg/g) | Bed utilization (%) |
| 6.5 | 24 | Straight | 4.0 | 4.67 | 4.41 | 19.17 |
| | | Helical coil—3 turns | 3.5 | 4.17 | 4.19 | 18.22 |
| | | Helical coil—6 turns | 4.1 | 4.83 | 4.46 | 19.39 |
| | 48 | Straight | 1.56 | 1.67 | 4.39 | 19.09 |
| | | Helical coil—3 turns | 1.25 | 1.33 | 4.13 | 17.96 |
| | | Helical coil—6 turns | 1.36 | 1.54 | 4.39 | 19.09 |
| | 100 | Straight | 0.69 | 0.71 | 5.69 | 24.74 |
| | | Helical coil—3 turns | 0.45 | 0.50 | 5.78 | 25.13 |
| | | Helical coil—6 turns | 0.46 | 0.51 | 5.66 | 24.61 |
| 13 | 24 | Straight | 1.22 | 1.33 | 5.91 | 25.70 |
| | | Helical coil—3 turns | 1.07 | 1.22 | 5.82 | 25.30 |
| | | Helical coil—6 turns | 1.18 | 1.33 | 5.89 | 25.61 |
| | 48 | Straight | 0.45 | 0.49 | 4.78 | 20.78 |
| | | Helical coil—3 turns | 0.42 | 0.46 | 4.9 | 21.30 |
| | | Helical coil—6 turns | 0.47 | 0.52 | 4.85 | 21.09 |
| | 100 | Straight | 0.10 | 0.18 | 5.62 | 24.43 |
| | | Helical coil—3 turns | 0.17 | 0.18 | 5.69 | 24.74 |
| | | Helical coil—6 turns | 0.17 | 0.18 | 6.01 | 26.13 |

[a]Breakthrough point: $[Zn^{2+}]_{outlet} = w \cdot [Zn^{2+}]_{feed}$.

batch conditions and 30˚C and pH 5. Therefore, the bed utilization (i.e. the ratio of bed capacity and batch capacity) ranged from 18 to 26%, see results reported in Table 2. These values are typical for dynamic adsorption/sorption process involved in heavy metal removal, e.g. [15].

The modeling of helical coil packed columns for $Zn^{2+}$ adsorption on bone char used Eq. (4) is included

in Fig. 2. Herein, it is convenient to remark that the modeling of breakthrough curves using mass transfer models is relatively more tedious and time consuming than the use of simplified models such as Thomas equation. However, the shape of breakthrough curves of $Zn^{2+}$ adsorption on bone char limits the application of Thomas, Bohart–Adams, Yoon–Nelson, Clark, Yang models, or other simplified breakthrough equations. For example, the Thomas equation failed to model the experimental breakthrough curves obtained in this study and showed low values of $R^2$ (results not reported for the sake of brevity). Overall, Eq. (4) is capable of describing satisfactorily the transient behavior of $Zn^{2+}$ concentration profile for the helical coil columns at tested operating conditions. Results of data fitting for experimental $Zn^{2+}$ breakthrough curves are reported in Table 3, which includes the adjustable parameters of the mass transfer model. Parameters $D_D$ and $K_p$ ranged from 155 to 455 $cm^2/s$ and 0.1 to 0.63 $m^3/kg$, respectively, for tested operating conditions. Overall, three-turn helical coil columns showed the highest values of axial dispersion $D_D$, see Table 3. In data fitting, the values of $R^2$ ranged from 0.95 to 0.99 where the modeling results were better for six-turn helical coil columns. The performance of the mass transfer model is worse in the zone $[Zn^{2+}]_{outlet}/[Zn^{2+}]_{feed} < 0.1$ of the breakthrough curves, while this model provides satisfactory predictions for $Zn^{2+}$ adsorption on bone char in the region $0.1 < [Zn^{2+}]_{outlet}/[Zn^{2+}]_{feed} < 1.0$. This mass transfer model is a reasonable approximation for data fitting of breakthrough curves of $Zn^{2+}$ adsorption on bone char using helical coil columns. In summary, this model can be used as a first approach for estimating the process dynamic and adsorption behavior in this column type and it is useful for performance analysis and design.

Fig. 4(a) shows the FTIR spectra of bone char used in $Zn^{2+}$ adsorption experiments. FTIR analysis showed the six characteristic bands of bone char: 3,420, 1,620, 1,450, 1,030, 600, and 565 $cm^{-1}$ [22,23]. The band at 3,420 $cm^{-1}$ corresponds to a high energy elongation peak from OH groups on the hydroxyapatite structure [24]. The characteristic bands of the phosphate group are observed at 1,030 and 600 $cm^{-1}$. They correspond to vibrations of the hydroxyapatite and are assigned to the stretching (1,030 $cm^{-1}$) and bending (600 $cm^{-1}$) vibrations of the phosphate group [23,25]. Finally, the absorption band at 565 $cm^{-1}$ corresponds to the calcium present in the inorganic structure of bone char [26]. Note that a new energy absorption band located at 450–510 $cm^{-1}$ is identified in the FTIR spectrum of metal-loaded adsorbent (BC-Zn), which could be attributed to the vibrational mode Zn–O in the matrix of bone char [27,28]. The presence of this new band could suggest the incorporation of $Zn^{2+}$ onto the bone char structure.

Table 3
Results of $Zn^{2+}$ breakthrough data correlation using mass transfer model

| | Operating conditions | | Mass transfer parameters | | |
|---|---|---|---|---|---|
| Feed flow, mL/min | $[Zn^{2+}]_{feed}$ (mg/L) | Bed geometry | $D_D$ ($cm^2/s$) | $K_p$ ($m^3/kg$) | $R^2$ |
| 6.5 | 24 | Straight | 155.28 | 1.0 | 0.99 |
| | | Helical coil—3 turns | 181.41 | 1.0 | 0.99 |
| | | Helical coil—6 turns | 134.17 | 1.0 | 0.98 |
| | 48 | Straight | 199.75 | 0.63 | 0.96 |
| | | Helical coil—3 turns | 235.43 | 0.63 | 0.99 |
| | | Helical coil—6 turns | 203.27 | 0.63 | 0.99 |
| | 100 | Straight | 389.45 | 0.35 | 0.96 |
| | | Helical coil—3 turns | 454.77 | 0.35 | 0.97 |
| | | Helical coil—6 turns | 443.72 | 0.35 | 0.98 |
| 13 | 24 | Straight | 179.4 | 0.44 | 0.98 |
| | | Helical coil—3 turns | 190.45 | 0.44 | 0.98 |
| | | Helical coil—6 turns | 172.36 | 0.44 | 0.99 |
| | 48 | Straight | 176.6 | 0.15 | 0.96 |
| | | Helical coil—3 turns | 184.42 | 0.15 | 0.97 |
| | | Helical coil—6 turns | 155.53 | 0.15 | 0.98 |
| | 100 | Straight | 377.89 | 0.12 | 0.96 |
| | | Helical coil—3 turns | 412.56 | 0.12 | 0.95 |
| | | Helical coil—6 turns | 325.13 | 0.12 | 0.97 |

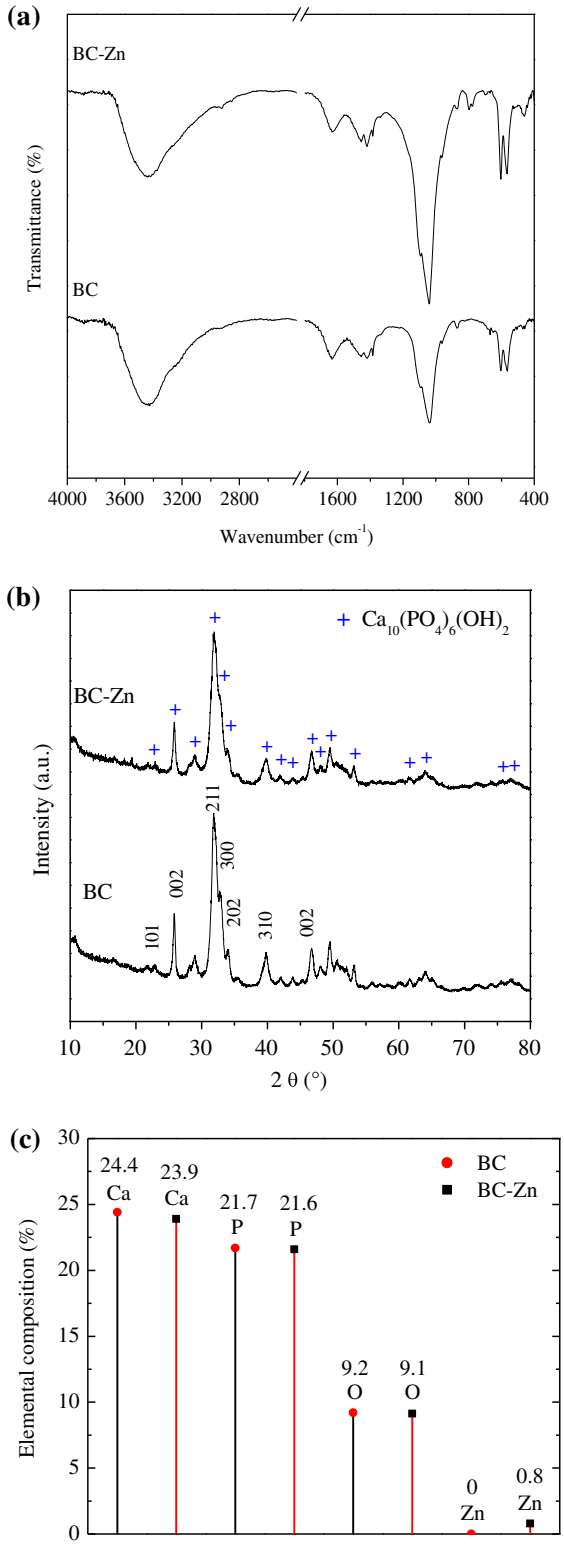


Fig. 4. (a) FTIR spectra, (b) XRD patterns, and (c) elemental composition by XRF analysis of bone char samples before (BC) and after zinc adsorption studies (BC-Zn).

On the other hand, Fig. 4(b) reports the XRD results for adsorbent samples. XRD diffraction peaks of adsorbent samples correspond to the crystalline structure of hydroxyapatite [$Ca_{10}(PO_4)_6(OH)_2$]. However, XRD results show that the characteristic reflections of the crystalline phase of the hydroxyapatite lost intensity after the $Zn^{2+}$ adsorption. It appears that $Zn^{2+}$ ions are adsorbed on the surface of hydroxyapatite of bone char via an ion exchange with $Ca^{2+}$ ions, leading to the formation of a new structure [$Ca_{10-x}Zn_x(PO_4)_6(OH)_2$]. Furthermore, $Zn^{2+}$ adsorption on the bone char surface caused that the hydroxyapatite lost its crystallinity. It is noteworthy that these results are consistent with data reported in the literature for heavy metal removal using bone char [17,29].

The elemental compositions (wt %) of bone char samples obtained by XRF analysis are reported in Fig. 4(c). This adsorbent is mainly constituted of calcium and phosphorus, 24.4 and 21.7%, respectively. Note that the calcium content of bone char decreased after $Zn^{2+}$ adsorption (i.e. from 24.4 to 23.9%). This result could be associated to the ion-exchange mechanism involved in the $Zn^{2+}$ removal. Finally, $Zn^{2+}$ is identified only in the metal-loaded sample (0.8%). On the other hand, XPS results are reported in Fig. 5. The oxygen deconvolution spectrum shows two important signals at 533.9 and 531.6 eV, which are associated with the interactions PO and OH, respectively [30,31]. These signals correspond to the phosphate group and the hydroxyl group in the structure of hydroxyapatite. In the region P 2p, a single signal is identified at 133.3 eV and it corresponds to the bond P–O of the phosphate group of the hydroxyapatite. Ca 2p XPS spectrum contains a single signal at 347.3 eV, which is characteristic of bond CaO [32]. Note that, after the $Zn^{2+}$ adsorption on bone char, an overlap occurs in the binding energy <0.4 eV for the regions O 1s, Ca 2p and P 2p. However, this phenomenon is not significant since the new binding energy formed corresponds to the same oxidation state of the element studied [32]. Finally, Zn 2p XPS spectrum for bone char samples show a signal at 1,022.8 eV that corresponds to the bond ZnO, which is formed between the oxygen from hydroxyapatite surface and adsorbed $Zn^{2+}$ ions [33]. According to Mendoza-Castillo et al. [17], the $Zn^{2+}$ adsorption on bone char could be attributed to the following mechanisms:

$$\equiv Ca^{2+} + M^{2+} = \equiv M^{2+} + Ca^{2+} \quad (6)$$

$$\equiv OH + M^{2+} = \equiv O - M^{+} + H^{+} \quad (7)$$

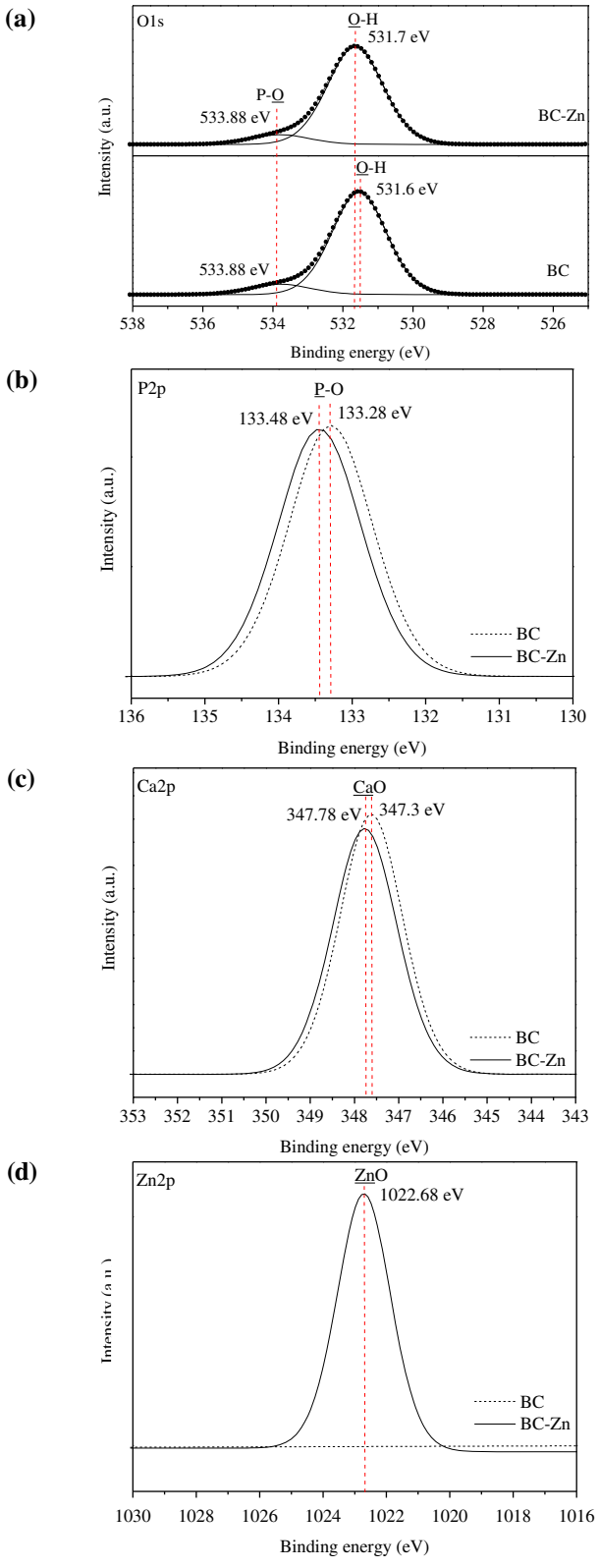


Fig. 5. Deconvolution of XPS spectra of bone char samples before (BC) and after zinc adsorption studies (BC-Zn). Spectrum: (a) O 1s, (b) P 2p, (c) Ca 2p, and (d) Zn 2p.

where $M^{2+}$ is the metal ion in aqueous solution and ≡ symbolizes the bone char surface, respectively.

## 4. Conclusions

This study introduces the application of helical coil columns for the liquid-phase adsorption at dynamic conditions. In particular, $Zn^{2+}$ adsorption on bone char has been performed using helical coil columns with different characteristics and a comparison has been conducted with respect to the results of conventional (i.e. straight) fixed-bed columns. Results showed that the helical coil adsorption columns may offer an equivalent removal performance than the traditional packed bed columns but using a compact structure. However, the coil diameter, number of turns, and feed flow appear to be crucial parameters for obtaining the best performance in this packed-bed geometry. On the other hand, a mass transfer model for a mobile fluid flowing through a porous media was successful for fitting and predicting the $Zn^{2+}$ breakthrough curves in helical coil bed columns. Finally, results of adsorbent physicochemical characterization showed that $Zn^{2+}$ adsorption on bone char can be attributed to an ion-exchange mechanism. In summary, helical coil columns appear to be a feasible configuration for large-scale adsorption systems with high flow rates where a significant reduction on purification system size can be obtained without compromising the adsorbent performance. Further studies should be focused on the optimization of this bed geometry for both mono- and multi-solutes systems.

## References

[1] J.L. Sotelo, A. Rodríguez, S. Álvarez, J. García, Removal of caffeine and diclofenac on activated carbon in fixed bed column, Chem. Eng. Res. Des. 90 (2012) 967–974.

[2] M.F.F. Sze, V.K.C. Lee, G. McKay, Simplified fixed bed column model for adsorption of organic pollutants using tapered activated carbon columns, Desalination 218 (2008) 323–333.

[3] O. Allahdin, S.C. Dehou, M. Wartel, P. Recourt, M. Trentesaux, J. Mabingui, A. Boughriet, Performance of FeOOH-brick based composite for Fe(II) removal from water in fixed bed column and mechanistic aspects, Chem. Eng. Res. Des. 91 (2013) 2732–2742.

[4] M.C. Basso, E.G. Cerrella, A.L. Cukierman, Activated carbons developed from a rapidly renewable biosource for removal of cadmium (II) and nickel (II) ions from dilute aqueous solutions, Ind. Eng. Chem. Res. 41 (2002) 180–189.

[5] L. Li, X. Li, J.Y. Lee, T.C. Keener, Z. Liu, X. Yao, The effect of surface properties in activated carbon on mercury adsorption, Ind. Eng. Chem. Res. 51 (2012) 9136–9144.
[6] M.R. Moreno-Virgen, R. Tovar-Gomez, D.I. Mendoza-Castillo, A. Bonilla-Petriciolet, Applications of activated carbons obtained from lignocellulosic materials for the wastewater treatment, in: V. Hernandez-Montoya, A. Bonilla-Petriciolet (Eds.), Lignocellulosic Precursors used in the Synthesis of Activated Carbon: Characterization Techniques and Applications in the Wastewater Treatment, first ed., 2012, Intech, 57–75.
[7] P.G. González, Y.B. Pliego-Cuervo. Adsorption of Cd(II), Hg(II) and Zn(II) from aqueous solution using mesoporous activated carbon produced from Bambusa vulgaris striata, Chem. Eng. Res. Des. 92 (2014) 2715–2724.
[8] I. Park, K.S. Knaebel, Adsorption breakthrough behavior: Unusual effects and possible causes, AIChE J. 38 (1992) 660–670.
[9] R. Tovar-Gómez, M.R. Moreno-Virgen, J.A. Dena-Aguilar, V. Hernández-Montoya, A. Bonilla-Petriciolet, M.A. Montes-Morán, Modeling of fixed-bed adsorption of fluoride on bone char using a hybrid neural network approach, Chem. Eng. J. 228 (2013) 1098–1109.
[10] A.A. Pota, A.P. Mathews, Adsorption dynamics in a stratified convergent tapered bed, Chem. Eng. Sci. 55 (2000) 1399–1409.
[11] M.F.F. Sze, G. McKay, Enhanced mitigation of parachlorophenol using stratified activated carbon adsorption columns, Water Res. 46 (2012) 700–710.
[12] M.F.F. Sze, G. McKay, Adsorptive removal of parachlorophenol using stratified tapered activated carbon column, Chin. J. Chem. Eng. 20 (2012) 444–454.
[13] H. Saffari, R. Moosavi, N.M. Nouri, C.X. Lin, Prediction of hydrodynamic entrance length for single and two-phase flow in helical coils, Chem. Eng. Process. Process Intensif. 86 (2014) 9–21.
[14] S.A. Nosier, M.M. Mohamed, Mass transfer at helical coils in bubble columns, Chem. Biochem. Eng. Q. 18 (2004) 235–239.
[15] I.A. Aguayo-Villarreal, A. Bonilla-Petriciolet, V. Hernández-Montoya, M.A. Montes-Morán, H.E. Reynel-Avila, Batch and column studies of $Zn^{2+}$ removal from aqueous solution using chicken feathers as sorbents, Chem. Eng. J. 167 (2011) 67–76.
[16] O. Abdelwahab, N.K. Amin, E.S.Z. El-Ashtoukhy, Removal of zinc ions from aqueous solution using a cation exchange resin, Chem. Eng. Res. Des. 91 (2013) 165–173.
[17] D.I. Mendoza-Castillo, A. Bonilla-Petriciolet, J. Jáuregui-Rincón, On the importance of surface chemistry and composition of bone char for the sorption of heavy metals from aqueous solution, Desalin. Water Treat. 54 (2015) 1651–1662.
[18] M. Germano, The Dean equations extended to a helical pipe flow, J. Fluid Mech. 203 (1989) 289–305.
[19] M.S. Shafeeyan, W.M.A.W. Wan Daud, A. Shamiri, A review of mathematical modeling of fixed-bed columns for carbon dioxide adsorption, Chem. Eng. Res. Des. 92 (2014) 961–988.
[20] K. You, H. Zhan, New solutions for solute transport in a finite column with distance-dependent dispersivities and time-dependent solute sources, J. Hydrology 487 (2013) 87–97.
[21] Y. Shao, H. Zhang, Y. Yan, Adsorption dynamics of p-nitrophenol in structured fixed bed with microfibrous entrapped activated carbon, Chem. Eng. J. 225 (2013) 481–488.
[22] C.K. Rojas-Mayorga, A. Bonilla-Petriciolet, I.A. Aguayo-Villarreal, V. Hernández-Montoya, M.R. Moreno-Virgen, R. Tovar-Gómez, M.A. Montes-Morán, Optimization of pyrolysis conditions and adsorption properties of bone char for fluoride removal from water, J. Anal. Appl. Pyrolysis 104 (2013) 10–18.
[23] C.K. Rojas-Mayorga, J. Silvestre-Albero, I.A. Aguayo-Villarreal, D.I. Mendoza-Castillo, A. Bonilla-Petriciolet, A new synthesis route for bone chars using $CO_2$ atmosphere and their application as fluoride adsorbents, Microporous Mesoporous Mater. 209 (2015) 38–44.
[24] F. Miyaji, Y. Kono, Y. Suyama, Formation and structure of zinc-substituted calcium hydroxyapatite, Mater. Res. Bull. 40 (2005) 209–220.
[25] C.A. Ogawa, A.M. de Guzzi Plepis. Preliminary studies of ciprofloxacin delivery in hydroxyapatite: Collagen composite, Rev. Bras. Engenharia Bioméd. 17 (2001) 123–130.
[26] S. Lurtwitayapont, T. Srisatit, Comparison of lead removal by various types of Swine bone adsorbents, Environ. Asia 3 (2010) 32–38.
[27] S. Bhaskar, P.S. Dobal, B.K. Rai, R.S. Katiyar, H.D. Bist, J.O. Ndap, A. Burger, Photoluminescence study of deep levels in Cr-doped ZnSe, J. Appl. Phys. 85 (1999) 439–443.
[28] J. Singh, P. Kumar, K.S. Hui, K.N. Hui, K. Ramam, R.S. Tiwari, O.N. Srivastava, Synthesis, band-gap tuning, structural and optical investigations of Mg doped ZnO nanowires, Cryst. Eng. Commun. 14 (2012) 5898–5904.
[29] K.K.H. Choy, G. McKay, Sorption of metal ions from aqueous solution using bone char, Environ. Int. 31 (2005) 845–854.
[30] G.D. Khattak, M.A. Salim, A.S. A1-Harthi, D.J. Thompson, L.E. Wenger, Structure of molybdenum-phosphate glasses by X-ray photoelectron spectroscopy (XPS), J. Non-Cryst. Solids 212 (1997) 180–191.
[31] P.Y. Shih, S.W. Yung, T.S. Chin, Thermal and corrosion behavior of $P_2O_5$-$Na_2O$-CuO glasses, J. Non-Cryst. Solids 224 (1998) 143–152.
[32] D. Briggs, M.P. Seah. Practical Surface Analysis: Ion and Neutral Spectroscopy, vol. 2, second ed., John Wiley and Sons, Chichester, 1993.
[33] G. Haemers, J.J. Verbist, S. Maroie, Surface oxidation of polycrystalline α(75%Cu/25%Zn) and β(53%Cu/47%Zn) brass as studied by XPS: Influence of oxygen pressure, Appl. Surf. Sci. 17 (1984) 463–467.